JACS
JOURNAL OF THE AMERICAN CHEMICAL SOCIETY
Article
pubs.acs.org/JACS

Pt Skin on AuCu Intermetallic Substrate: A Strategy to Maximize Pt Utilization for Fuel Cells

Gongwei Wang,[†] Bing Huang,[†] Li Xiao,*[,†] Zhandong Ren,[†] Hao Chen,[‡] Deli Wang,[‡] Héctor D. Abruña,*[,‡] Juntao Lu,[†] and Lin Zhuang*[,†]

[†]College of Chemistry and Molecular Sciences, Hubei Key Lab of Electrochemical Power Sources, Wuhan University, Wuhan 430072, P.R. China

[‡]Department of Chemistry and Chemical Biology, Baker Lab, Cornell University, Ithaca, New York 14853-1301, United States

Supporting Information

ABSTRACT: The dependence on Pt catalysts has been a major issue of proton-exchange membrane (PEM) fuel cells. Strategies to maximize the Pt utilization in catalysts include two main approaches: to put Pt atoms only at the catalyst surface and to further enhance the surface-specific catalytic activity (SA) of Pt. Thus far there has been no practical design that combines these two features into one single catalyst. Here we report a combined computational and experimental study on the design and implementation of Pt-skin catalysts with significantly improved SA toward the oxygen reduction reaction (ORR). Through screening, using density functional theory (DFT) calculations, a Pt-skin structure on AuCu(111) substrate, consisting of 1.5 monolayers of Pt, is found to have an appropriately weakened oxygen affinity, in comparison to that on Pt(111), which would be ideal for ORR catalysis. Such a structure is then realized by substituting the Cu atoms in three surface layers of AuCu intermetallic nanoparticles (AuCu *i*NPs) with Pt. The resulting Pt-skinned catalyst (denoted as Pt^{S}AuCu *i*NPs) has been characterized in depth using synchrotron XRD, XPS, HRTEM, and HAADF-STEM/EDX, such that the Pt-skin structure is unambiguously identified. The thickness of the Pt skin was determined to be less than two atomic layers. Finally the catalytic activity of Pt^{S}AuCu *i*NPs toward the ORR was measured via rotating disk electrode (RDE) voltammetry through which it was established that the SA was more than 2 times that of a commercial Pt/C catalyst. Taking into account the ultralow Pt loading in Pt^{S}AuCu *i*NPs, the mass-specific catalytic activity (MA) was determined to be 0.56 A/mg$_{Pt}$@0.9 V, a value that is well beyond the DOE 2017 target for ORR catalysts (0.44 A/mg$_{Pt}$@0.9 V). These findings provide a strategic design and a realizable approach to high-performance and Pt-efficient catalysts for fuel cells.

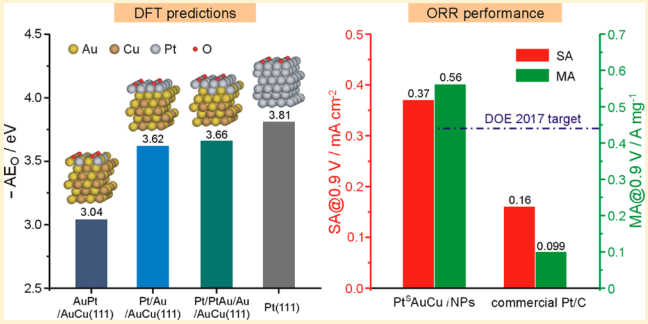

INTRODUCTION

Despite being a clean and efficient power source suitable for automotive applications, proton exchange membrane fuel cells (PEMFCs) have not been widely deployed, in part because of the heavy use, and often limited lifetime, of Pt catalyst for accelerating the sluggish oxygen reduction reaction (ORR).[1−3] How to minimize the Pt loading in PEMFCs has been the subject of fundamental and technological significance for the past decades.[4−7] The ultimate solution to this issue would rely on two approaches: to put Pt atoms only on the catalyst surface[8,9] and to tune the Pt surface to be more catalytically efficient for the ORR.[10,11] Ideally, these two features would be combined into a single catalyst, namely, a Pt-skin structure with enhanced catalytic activity.[12−14] Such a strategy requires not only a controllable synthesis of the desired nanostructure but also a proper choice of the catalyst substrate that can promote and stabilize the Pt skin.[15,16]

On the one hand, there are a number of physical and/or chemical methods for making Pt thin films. Vapor deposition approaches, such as thermal evaporation[17,18] and atomic layer deposition (ALD),[19−21] depend on special apparatus and are not generally designed for powder preparation, while chemical methods, such as seeding growth,[22−24] are usually not good at precise control of epitaxial growth. The most popular approach for obtaining a Pt monolayer on certain flat substrates is the underpotential deposition (UPD) of Cu followed by galvanic displacement.[15] However, it has to be done under electrochemical conditions and usually cannot achieve a full coverage of Pt on nanoparticles.[25,26] An adequate, practical and scalable synthetic method for nanoparticles, with a well-defined Pt-skin structure, has hitherto been lacking.

On the other hand, the choice of the proper substrate, which can promote the catalytic activity of the Pt skin, is still not clear. For the ORR, ordinary bulk Pt surface binds oxygenated intermediates too strongly;[27,28] thus, a general strategy for improving the catalytic activity of Pt toward the ORR is to lower the surface oxygen affinity of Pt to certain degree.[29]

Received: April 2, 2014
Published: June 17, 2014

dx.doi.org/10.1021/ja503315s | J. Am. Chem. Soc. 2014, 136, 9643−9649

Theoretical calculations have predicted that lowering the oxygen adsorption energy (AE_O) by 0.2 eV could result in the best performance.[30,31] Therefore, it would be ideal to identify/develop a catalyst substrate that is not only suitable for Pt coating but also able to slightly suppress the binding affinity of oxygen intermediates of the Pt skin.

In the present work, we report our combined computational and experimental study on maximizing the Pt utilization and enhancing ORR activity for fuel cells. Based on a survey, using density functional theory (DFT) calculations, we have found that a Pt skin (1−2 monolayers thick) on a AuCu intermetallic substrate, would be an ideal structure, on which the AE_O can be decreased, relative to that on Pt(111), to an extent close to 0.2 eV. Furthermore, this Pt/AuCu structure can be readily implemented in the form of nanocatalysts via a simple chemical procedure. Upon mixing AuCu intermetallic nanoparticles (AuCu *i*NPs) with a Pt(II) solution, a uniform Pt skin can be spontaneously formed in a controllable fashion.

In a previous study, we reported on a surfactant-free synthesis of AuCu *i*NPs,[32] onto which we now fabricate the Pt skin. The resulting catalyst has been comprehensively characterized using synchrotron X-ray techniques and high-resolution scanning transmission electron microscopy (STEM). The catalytic activity of this material toward the ORR (0.56 A/mg_{Pt}@0.9 V) was determined to be well above the DOE 2017 target (0.44 A/mg_{Pt}@0.9 V) for Pt-based cathode catalysts for PEMFCs.[33]

COMPUTATIONAL AND EXPERIMENTAL SECTION

Density Functional Theory (DFT) Calculations. DFT calculations were performed using the Vienna Atomic Simulation Package (VASP, version 5.3)[34,35] within an RPBE generalized gradient approximation (GGA) to the exchange and correlation functional.[36] A projected augmented wave (PAW) basis, along with a plane-wave kinetic energy cutoff of 408 eV, was used throughout. For the calculations of surface and chemisorption systems, a $p(2 \times 2)$ surface unit cell (corresponding to 1/4 surface coverage) was used to construct a six-layer metal slab and repeated in super cell geometry with successive slabs separated by a vacuum region equivalent to six metal layers, and the Brillouin zone was sampled using a $6 \times 6 \times 1$ Monkhorst−Pack mesh.[37] During the geometry optimization, the adsorbate layer and the top three layers of the slab were allowed to relax. The energies were converged to 1 meV per atom, and ionic relaxations were allowed until the absolute value of force on each atom was below 0.02 eV/Å.

Preparation of Pt-Skin AuCu Intermetallic Nanoparticles (Pt^SAuCu *i*NPs). Carbon-supported AuCu intermetallic nanoparticles (AuCu *i*NPs) were synthesized as reported in our earlier paper.[32] The diameter of the AuCu *i*NPs was measured by both X-ray diffraction (XRD) and transmission electron microcopy (TEM). The specific surface area of AuCu *i*NPs could then be estimated and the amount of Pt precursor necessary to displace the surface Cu component of the AuCu *i*NPs calculated. To produce the Pt skin, carbon-supported AuCu *i*NPs (40 wt %, 8 mg) were dispersed in an aqueous solution containing the desired amount of K_2PtCl_4 (~5 μmol) at room temperature by thoroughly stirring and ultrasonic blending several times. The mixture was then stirred overnight (about 12 h). Finally, the resulting Pt-skin AuCu intermetallic nanoparticles (Pt^SAuCu *i*NPs) were separated by centrifugation from the solution, washed three times with ultrapure water, and dried in vacuum. X-ray fluorescence analysis (XRF, Shimadzu EDX-720) was employed to determine the amount of residual K_2PtCl_4 and the $CuCl_2$ produced in the filtrate. These data were used to verify the Pt loading in Pt^SAuCu *i*NPs. All chemicals used in the present work were of at least analytical grade.

Material Characterizations. Synchrotron X-ray diffraction (XRD) patterns of the catalyst powder were collected at the beamline BL02B2 (Spring-8 in Japan), equipped with a large Debye−Scherrer camera. Powder samples were filled in a glass capillary and sealed with a resin. To minimize the effect of X-ray absorption by the samples, the wavelength of the incident X-ray beam was set to 0.50005 Å using a Si monochromator, which was calibrated with a CeO_2 standard. XRD data were recorded on an imaging plate for 30 min in the range 2θ = 0°−75° with a 2θ step of 0.01°. X-ray photoelectron spectroscopy (XPS) measurements were carried out using a Kratos XSAM-800 spectrometer with an Mg Kα radiation source. High-resolution transmission electron microscopy (HRTEM) observations were conducted on a JEOL JEM2010FEF operated at 200 keV. High resolution scanning transmission electron microscopy/energy dispersive X-ray microanalysis (HRSTEM/EDX) were performed on a Tecnai F20 equipped with Shottky field-emission gun operated at 200 keV with an installed monochromator.

Electrochemical Measurements. To prepare the working electrode, 2 mg of catalyst powder were dispersed ultrasonically in 0.4 mL of a Nafion (0.05 wt %) alcohol solution to form an ink, and 10 μL of the ink were pipetted onto a glassy carbon (GC) substrate (ϕ = 5 mm), which had been buff-polished with an alumina suspension (ϕ = 0.05 μm) prior to use. The catalyst-coated electrode was dried under an infrared lamp before electrochemical tests. Electrochemical experiments were conducted on a CHI-660 potentiostat with a rotating disk electrode (RDE) system (Pine Research Instruments) at 25 °C. Cyclic voltammetry (CV) was carried out in a deaerated 0.5 M H_2SO_4 solution. A sheet of graphite paper (Toray) was used as the counter electrode. The reference electrode was a reversible hydrogen electrode (RHE) in the same solution. CO stripping experiments were conducted under the same conditions as CV measurements except that the working electrode surface was preadsorbed with CO. The CO adsorption procedure was accomplished by polarizing the electrode at 0.1 V (vs RHE) and bubbling the solution with CO for 10 min and subsequently with Ar for another 10 min. The ORR measurements were carried out in an O_2-saturated 0.1 M $HClO_4$ solution. The rotation rate was 900 rpm, and the ORR polarization curves were recorded by scanning the potential from 0.3 to 1.1 V (vs RHE) at 5 mV/s. All solutions were prepared using ultrapure water (18 MΩ·cm), and all measurements were conducted at 25 °C.

RESULTS AND DISCUSSION

Theoretical Considerations of a AuCu(111) Surface with a Pt Skin. Using DFT, one can predict the type of Pt-skin surface that would exhibit enhanced performance for ORR catalysis.[38] The criterion employed here was the oxygen adsorption energy (AE_O), a descriptor that correlates very well with the catalytic activity of Pt toward the ORR.[39−41] In the present work, AuCu(111) surfaces with Pt skins of different thickness were constructed by displacing the Cu atoms at the top one to three layers, with Pt atoms. As shown in Figure 1, the Cu atoms at the first layer are displaced with Pt, the topmost surface becomes PtAu, on which the AE_O is −3.04 eV, much smaller (in absolute value) than the value for bulk Pt(111) (AE_O = −3.81 eV). When the Cu atoms at the top two layers are displaced, the AE_O does not change much, but if a segregation of Pt occurs (i.e., a pure Pt first (topmost) layer and a pure Au second layer), the AE_O will be −3.62 eV. This value is smaller than that of bulk Pt(111) by 0.19 eV, very close to the expected optimal shift (0.2 eV).[30,31] When the Cu atoms are displaced from the top three layers, the AE_O of the Pt segregated surface (corresponding to 1.5 monolayers of Pt) is −3.66 eV, 0.15 eV smaller in AE_O than bulk Pt(111), which is still close to the optimal value.

While the above theoretical considerations are based on ideal and periodic surfaces and may not exactly correspond to the real surface structure of nanocatalysts, they do provide a clear indication that one or two monolayers of Pt on a AuCu intermetallic substrate could be the structure we have been

dx.doi.org/10.1021/ja503315s | J. Am. Chem. Soc. 2014, 136, 9643−9649

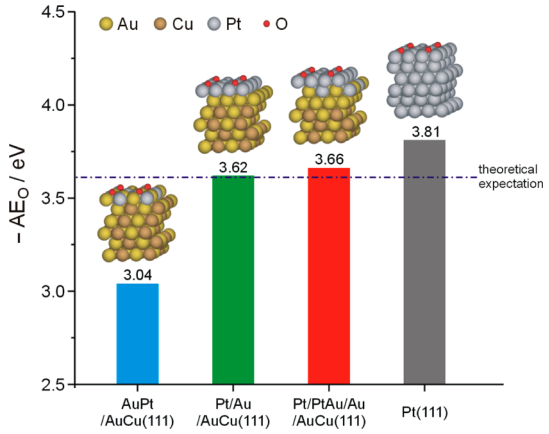

Figure 1. DFT-calculated oxygen adsorption energy (AE_O) for AuCu(111) surfaces covered with different thickness of Pt skin (obtained by displacing the Cu atoms in the top first to third surface layers and segregating Pt at the surface). Result for Pt(111) is presented for comparison.

seeking, namely, a Pt-skin surface with optimal oxygen affinity for ORR catalysis.

Experimental Implementation of a Pt Skin on AuCu Intermetallic Nanoparticles. In reality, however, the Cu−Pt displacement reaction cannot proceed in perfect registry, given the mismatch in atomic size and the irregular morphology of nanoparticles. We found that at least 2−3 surface layers of Cu displacement are necessary to form a stable Pt skin on AuCu *i*NPs and to protect the inner Cu atoms from leaching under electrochemical conditions (vide infra). In the following, we present results for materials in which three layers of Cu were displaced, which is expected to produce a Pt skin with an average thickness of 1.5 monolayers (see the corresponding model in Figure 1).

The AuCu *i*NPs before and after Pt displacement were first characterized using X-ray techniques. From the XRD patterns (Figure 2a), the tetragonal AuCu crystalline structure can be clearly identified for AuCu *i*NPs with or without a Pt skin, and the crystalline size was calculated (based on the AuCu(311) reflection) to be ∼6 nm. No signals associated with a Pt phase were observed in Pt^{S}AuCu *i*NPs. Note that the synchrotron XRD has sufficient sensitivity that even small local Pt phases on the catalyst surface, if any, would be detectable. The absence of an XRD signal for Pt indicates that the Pt skin has the same lattice structure as the AuCu intermetallic substrate.

However, the Pt skin can be detected by XPS. As shown in Figure 2b, the pair of Pt 4f signals is well resolved from the background of Au 4f signals. More importantly, the chemical properties of the Pt skin is distinctly different from that of a conventional Pt/C catalyst. There is a large negative shift (0.74 eV) in the binding energy, indicating that the Pt skin has accepted a partial charge transferred from the AuCu intermetallic substrate, which would lower the *d*-band reactivity as well as the surface oxygen affinity.[42,43]

Electron Microscopic Observation of Pt^{S}AuCu *i*NPs. To gain spatially resolved compositional information on the AuCu *i*NPs before and after Pt displacement, high-resolution electron microscopic observations were employed. From the TEM images (Figure 3), one can see that the morphology of the AuCu *i*NPs is approximately spherical (Figure 3a) and remains essentially unchanged after Pt displacement (Figure 3b) and that no Pt dendrites appear on the surface of AuCu

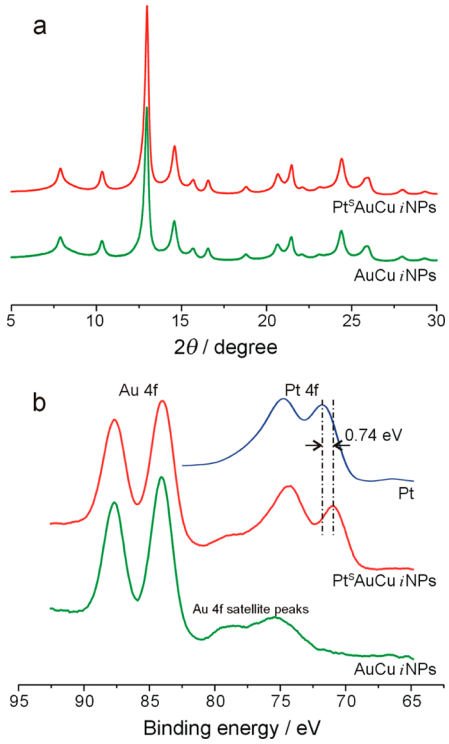

Figure 2. Synchrotron X-ray diffraction patterns (a) and X-ray photoelectron spectra (b) for the studied nanocatalysts.

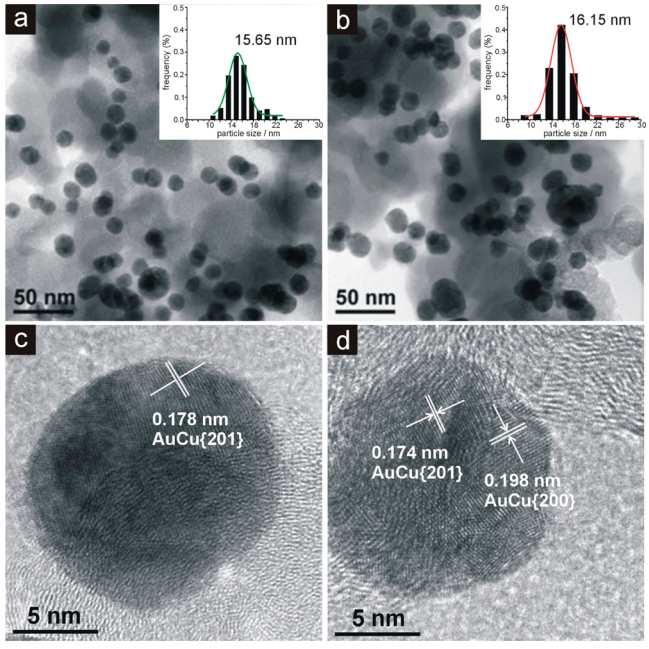

Figure 3. TEM micrographs and the corresponding histograms of the particle size distribution (insets) of AuCu *i*NPs (a) and Pt^{S}AuCu *i*NPs (b), and HRTEM micrographs of an individual particle for AuCu *i*NPs (c) and Pt^{S}AuCu *i*NPs (d).

*i*NPs (a situation often seen in conventional seeding growth). On the basis of a statistical analysis over hundreds of particles, the average particle size of the AuCu *i*NPs was determined to be 15.7 nm, and after Pt displacement, the particle size appears to increase slightly to 16.2 nm, which is understandable and anticipated given that Pt is larger in atomic size than Cu. Such a slight expansion in particle size is not due to a penetration of Pt

dx.doi.org/10.1021/ja503315s | J. Am. Chem. Soc. 2014, 136, 9643−9649

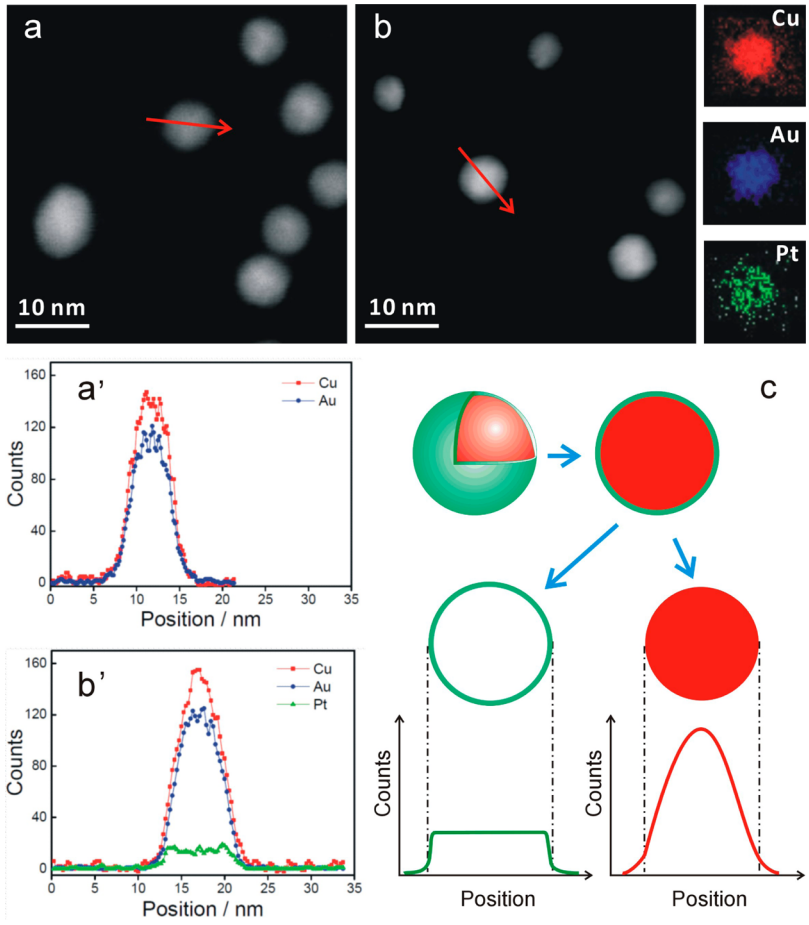

Figure 4. HAADF-STEM images of AuCu *i*NPs (a) and Pt^{S}AuCu *i*NPs (b) with EDX element mapping. (a′) and (b′) are corresponding STEM-EDX line scans in (a) and (b), respectively. (c) Schematic illustration of the STEM-EDX line shapes for the skin component and the core component.

atoms into the core of the AuCu *i*NPs. Close observations (Figure 3c) reveal that the highly ordered structure inside the AuCu *i*NPs has remained unchanged after Pt displacement (Figure 3d), which is consistent with the XRD results. The above TEM observations indicate that the Pt displacement occurred only at the surface without changing either the morphology or the bulk structure of the AuCu *i*NPs. Such an advantageous feature should result from the relatively uniform surface property and the ordered bulk structure provided by the intermetallic substrate.

To unambiguously identify the Pt skin, we employed high-angle annular dark-field scanning transmission electron microscopy (HAADF-STEM), in conjunction with EDX analysis, to achieve elemental mapping over a single catalyst nanoparticle. As shown in Figure 4, while the STEM images of AuCu *i*NPs and Pt^{S}AuCu *i*NPs appear essentially identical, the element map of Pt is distinct from those of Au and Cu. The line profiles of Au and Cu in both AuCu *i*NPs and Pt^{S}AuCu *i*NPs take on a bell shape (Figure 4a′ and b′), typical for solid and spherical particles (Figure 4c). In contrast, the line profile for Pt over Pt^{S}AuCu *i*NP shows a plateau with a much lower height, indicating that the Pt must be uniformly distributed in a very thin shell (Figure 4c). Note that in literature reports of core–shell structured nanoparticles a valley shape can often be seen for the line profile of the shell element, which is due to the much thicker shell, in comparison to the present case.

Surface Composition of Pt^{S}AuCu *i*NPs. Now that the Pt-skin structure of Pt^{S}AuCu *i*NPs has been confirmed, further information about the surface composition, such as the thickness and the Pt/Au ratio of the Pt skin, can be assessed by the amount of Pt loaded and the electrochemical surface area (ESA) of Pt. As mentioned in the Computational and Experimental Section, the Pt loading of Pt^{S}AuCu *i*NPs was established on the basis of the amount of residual K_2PtCl_4 and $CuCl_2$ produced in the filtrate, measured by XRF. The metal weight percentage of the carbon-supported Pt^{S}AuCu *i*NPs has been determined to be 2.8 wt % Pt and 39 wt % AuCu.

The ESA of Pt was obtained by the CO stripping method, where CO molecules adsorb only on surface Pt atoms and the CO oxidation charge can be converted into a surface area by a conversion factor of 420 μC/cm^2.[44] The CO stripping curve for Pt^{S}AuCu *i*NPs is presented in Figure 5a, and compared to that of a commercial Pt/C catalyst (Figure 5b). Given the total amount of Pt on the electrode, the ESA of Pt is calculated to be 150 cm^2/g for Pt^{S}AuCu *i*NPs and 62 cm^2/g for the commercial Pt/C catalyst.[45] Since the theoretical maximum ESA of Pt is 237 cm^2/g (a case in which all Pt atoms are accessible),[46] the Pt atoms exposed at the outmost surface of the Pt^{S}AuCu *i*NPs are estimated to be ~63% of the total amount of Pt atoms. In other words, the thickness of the Pt skin of Pt^{S}AuCu *i*NPs should be less than two atomic layers as expected from the experimental control where a three-layer displacement of surface Cu atoms

dx.doi.org/10.1021/ja503315s | J. Am. Chem. Soc. 2014, 136, 9643–9649

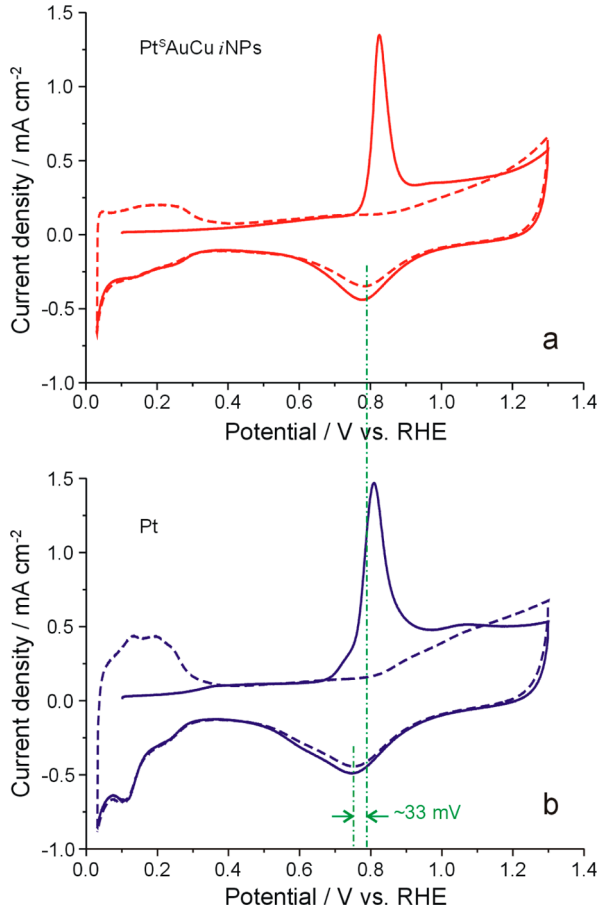

Figure 5. CO stripping curves of Pt^{S}AuCu *i*NPs (a) and commercial Pt/C (b) in 0.5 M H_2SO_4 at a scan rate 20 mV/s.

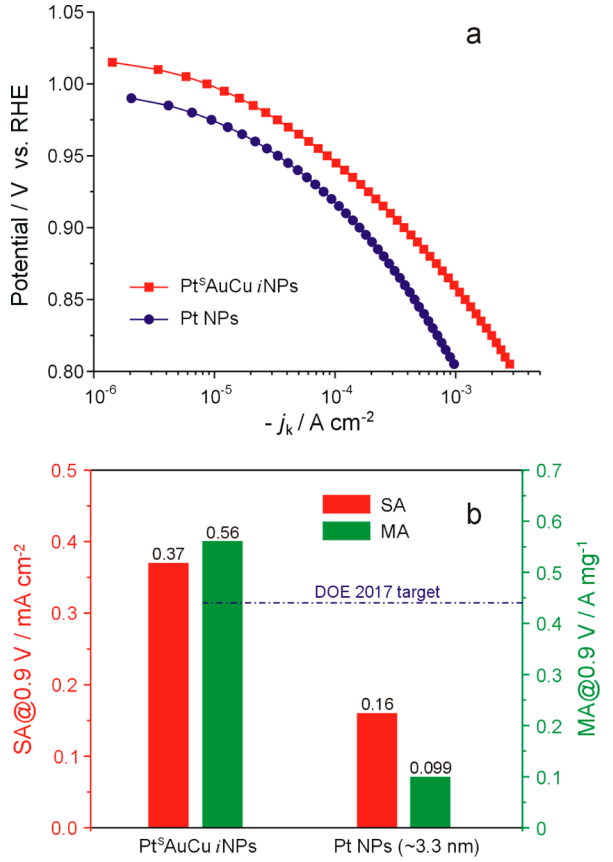

Figure 6. ORR catalysis of Pt^{S}AuCu *i*NPs and commercial Pt/C in O_2-saturated 0.1 M $HClO_4$ solution. (a) Tafel plots. The kinetic current density (j_k) is normalized to the ESA of Pt obtained in a CO stripping experiment. (b) Comparisons in surface-specific catalytic activity (SA) and mass-specific catalytic activity (MA) at 0.9 V (vs RHE).

would result in 1.5 monolayers of Pt if segregation occurred (Figure 1).

The CV of Pt^{S}AuCu *i*NPs (Figure S1 in the Supporting Information [SI]) reveals that there is no Cu at the surface, and the Pt/Au ratio at the outmost surface was assessed, on the basis of the reduction charges of surface oxides, to be 82:18. Since the global Pt/Au ratio in the Pt skin should be 1:1, the segregation of Pt atoms on the outmost surface is evident. Such a structure is qualitatively consistent with the theoretical model used in the DFT calculations (Figure 1).

Catalytic Activity of Pt^{S}AuCu *i*NPs toward the ORR. Also revealed from the electrochemical behavior of Pt^{S}AuCu *i*NPs (Figure 5) is the fact that the reduction potential of surface oxides shifts positively by ~33 mV, with respect to Pt/C. This is a good indication that the oxygen affinity of Pt has been weakened,[47,48] as predicted by DFT calculations, and that the catalytic activity of Pt^{S}AuCu *i*NPs toward the ORR should be concomitantly improved. Evaluations of the ORR catalytic activity were performed using the RDE technique (Figure S2 in the SI), and the resulting polarization curves (potential versus kinetic current density) are plotted in Figure 6a. Compared to the commercial Pt/C catalyst, the Pt^{S}AuCu *i*NPs is clearly superior in catalyzing the ORR. At 0.9 V (vs RHE), the surface-specific activity (SA) of Pt^{S}AuCu *i*NPs is 0.37 mA/cm^2, more than twice that of Pt/C (0.16 mA/cm^2). Considering that the Pt loading of Pt^{S}AuCu *i*NPs (1.4 μg) is much lower than that of Pt/C (5 μg), the improvement in mass-specific activity (MA) is dramatic. As presented in Figure 6b, the MA of Pt^{S}AuCu *i*NPs at 0.9 V is 0.56 A/mg$_{Pt}$, which is more than 5 times the MA of Pt/C (0.099 A/mg$_{Pt}$). Moreover this value surpasses the DOE 2017 target,[33] a MA for Pt at 0.9 V of 0.44 A/mg$_{Pt}$ at 80 °C under IR-free conditions. The catalytic stability of Pt^{S}AuCu *i*NPs was tested by cycling the electrode potential over the range of 0.6−1.1 V in O_2 saturated $HClO_4$ solution. After 10,000 cycles, the MA of Pt^{S}AuCu *i*NPs at 0.9 V remained at 0.4 A/mg$_{Pt}$, which is still over 4 times the MA of fresh Pt/C.

On the basis of the above computational and experimental results, we believe that the improvement in the catalytic activity of Pt^{S}AuCu *i*NPs toward the ORR is largely the result of the special structure and electronic properties of the Pt skin. The relatively small lattice constant of the AuCu substrate will lead to a compressive strain in the Pt skin, and the surface Au atoms, albeit to a smaller extent, will affect the reactivity of Pt via the ligand effect. Both of these electronic effects lower the surface reactivity of Pt and reduce the oxygen affinity to an appropriate degree so as to enhance electrocatalytic activity. Note that, under this mechanism, the particle size of the intermetallic core is not a key factor for improving the catalytic activity or the Pt utilization. In fact, further reduction in the crystalline size of AuCu *i*NPs would be at the risk of losing the ordered structure.[49]

■ CONCLUSIONS

We find that a Pt skin, consisting of 1.5 monolayers of Pt, on a AuCu intermetallic substrate core is a realizable structure that is

dx.doi.org/10.1021/ja503315s | J. Am. Chem. Soc. 2014, 136, 9643−9649

not only efficient in the utilization of Pt but also highly active for the ORR. DFT calculations predicted that a Pt/AuCu(111) surface would have the appropriate oxygen affinity to enhance electrocatalytic activity. Namely, the oxygen adsorption energy (AE_O) is lower than that on Pt(111) by close to 0.2 eV, the theoretically expected optimal value for ORR catalysis. Such a Pt-skin structure can be readily implemented in the form of nanocatalysts by displacing the surface Cu atoms on AuCu intermetallic nanoparticles (AuCu *i*NPs) with Pt. The resulting Pt-skinned catalyst (denoted as Pt^SAuCu *i*NPs) has been thoroughly characterized using synchrotron X-ray and high-resolution electron microscopies. The Pt-skin structure of Pt^SAuCu *i*NPs has been unambiguously identified and is consistent with theoretical expectation. The thickness of the Pt skin was determined to be less than 2 atomic layers, and over 60% of the Pt atoms are segregated to the outmost surface of the nanoparticles. The modified electronic properties of the Pt skin are evident in XPS and electrochemical measurements. The surface catalytic activity (SA) of Pt^SAuCu *i*NPs toward the ORR was found to be more than twice that of a commercial Pt/C catalyst. Because of the ultralow Pt loading of this Pt-skinned catalyst, the mass-specific catalytic activity (MA) of Pt^SAuCu *i*NPs toward the ORR reached 0.56 A/mgPt@0.9 V. Not only is this more than 5 times that of Pt/C, but it is also well beyond the DOE 2017 target for ORR catalysts (0.44 A/mg_{Pt}@0.9 V).

The present work has demonstrated a successful combination of computational and experimental studies on ORR catalyst design, and shown that it is possible to achieve higher catalytic activity with less Pt, using well-defined and controllable Pt-skin structures with the appropriate core. These findings provide not only strategic considerations but also a realistic methodology for the development of Pt-efficient catalysts for fuel cells.

■ ASSOCIATED CONTENT

Supporting Information

Figures S1 and S2. This material is available free of charge via the Internet at http://pubs.acs.org.

■ AUTHOR INFORMATION

Corresponding Authors

chem.lily@whu.edu.cn
hda1@cornell.edu
lzhuang@whu.edu.cn

Notes

The authors declare no competing financial interest.

■ ACKNOWLEDGMENTS

This work was financially supported by the National Basic Research Program (2012CB932800, 2012CB215500), the National Science Foundation of China (20933004, 21125312, 21203142), the National Hi-Tech R&D Program (2011AA050705), Program for Changjiang Scholars and Innovative Research Team in University (IRT1030), and the Doctoral Fund of Ministry of Education of China (20110141130002). We are grateful to Dr. Xiaoming Wang and Prof. Yoshiharu Uchimoto at Kyoto University for the synchrotron experiments. This work was supported in part by the Energy Materials Center at Cornell (emc^2), an Energy Frontier Research Center funded by the U.S. Department of Energy, Office of Science, Office of Basic Energy Sciences under Award Number DE-SC0001086. This work made use of the electron microscopy facility of the Cornell Center for Materials Research (CCMR) with support from the National Science Foundation Materials Research Science and Engineering Centers (MRSEC) Program (DMR 1120296).

■ REFERENCES

(1) Steele, B. C. H.; Heinzel, A. *Nature* **2001**, *414*, 345−352.
(2) Vielstich, W.; Lamm, A.; Gasteiger, H. A. *Handbook of Fuel Cells: Fundamentals, Technology, Applications*; Wiley: New York, 2003; Vol. 3.
(3) Debe, M. K. *Nature* **2012**, *486*, 43−51.
(4) Stamenkovic, V.; Mun, B. S.; Arenz, M.; Mayerhofer, K. J. J.; Lucas, C. A.; Wang, G.; Ross, P. N.; Markovic, N. *Nat. Mater.* **2007**, *6*, 241−247.
(5) Stamenkovic, V. R.; Fowler, B.; Mun, B. S.; Wang, G.; Ross, P. N.; Lucas, C. A.; Markovic, N. M. *Science* **2007**, *315*, 493−497.
(6) Gasteiger, H. A.; Kocha, S. S.; Sompali, B.; Wagner, F. T. *Appl. Catal., B* **2005**, *56*, 9−35.
(7) Wee, J.-H.; Lee, K.-Y.; Kim, S. H. *J. Power Sources* **2007**, *165*, 667−677.
(8) Sasaki, K.; Wang, J. X.; Naohara, H.; Marinkovic, N.; More, K.; Inada, H.; Adzic, R. R. *Electrochim. Acta* **2010**, *55*, 2645−2652.
(9) Wang, D.; Xin, H. L.; Yu, Y.; Wang, H.; Rus, E.; Muller, D. A.; Abruña, H. D. *J. Am. Chem. Soc.* **2010**, *132*, 17664−17666.
(10) Wu, J. B.; Yang, H. *Acc. Chem. Res.* **2013**, *46*, 1848−1857.
(11) Zhang, J. L.; Vukmirovic, M. B.; Sasaki, K.; Nilekar, A. U.; Mavrikakis, M.; Adzic, R. R. *J. Am. Chem. Soc.* **2005**, *127*, 12480−12481.
(12) Nilekar, A. U.; Mavrikakis, M. *Surf. Sci.* **2008**, *602*, L89−L94.
(13) Wang, J. X.; Inada, H.; Wu, L.; Zhu, Y.; Choi, Y.; Liu, P.; Zhou, W.-P.; Adzic, R. R. *J. Am. Chem. Soc.* **2009**, *131*, 17298−17302.
(14) Ghosh, T.; Vukmirovic, M. B.; DiSalvo, F. J.; Adzic, R. R. *J. Am. Chem. Soc.* **2010**, *132*, 906−907.
(15) Adzic, R. R.; Zhang, J.; Sasaki, K.; Vukmirovic, M. B.; Shao, M.; Wang, J. X.; Nilekar, A. U.; Mavrikakis, M.; Uribe, F. *Top. Catal.* **2007**, *46*, 249−262.
(16) Sasaki, K.; Naohara, H.; Choi, Y. M.; Cai, Y.; Chen, W.-F.; Liu, P.; Adzic, R. R. *Nat. Commun.* **2012**, *3*, 1115.
(17) Esposito, D. V.; Hunt, S. T.; Stottlemyer, A. L.; Dobson, K. D.; McCandless, B. E.; Birkmire, R. W.; Chen, J. G. *Angew. Chem., Int. Ed.* **2010**, *49*, 9859−9862.
(18) Esposito, D. V.; Hunt, S. T.; Kimmel, Y. C.; Chen, J. G. *J. Am. Chem. Soc.* **2012**, *134*, 3025−3033.
(19) Jiang, X.; Gür, T. M.; Prinz, F. B.; Bent, S. F. *Chem. Mater.* **2010**, *22*, 3024−3032.
(20) An, J.; Kim, Y.-B.; Prinz, F. B. *Phys. Chem. Chem. Phys.* **2013**, *15*, 7520−7525.
(21) Aaltonen, T.; Ritala, M.; Sajavaara, T.; Keinonen, J.; Leskela, M. *Chem. Mater.* **2003**, *15*, 1924−1928.
(22) Peng, Z.; Yang, H. *J. Am. Chem. Soc.* **2009**, *131*, 7542−7543.
(23) (a) Wang, L.; Yamauchi, Y. *J. Am. Chem. Soc.* **2010**, *132*, 13636−13638. (b) Wang, L.; Yamauchi, Y. *Chem. Mater.* **2011**, *23*, 2457−2465. (c) Ataee-Esfahani, H.; Imura, M.; Yamauchi, Y. *Angew. Chem., Int. Ed.* **2013**, *52*, 13611−13615.
(24) (a) Lim, B.; Jiang, M. J.; Camargo, P. H. C.; Cho, E. C.; Tao, J.; Lu, X. M.; Zhu, Y. M.; Xia, Y. N. *Science* **2009**, *324*, 1302−1305. (b) Lim, B.; Jiang, M.; Yu, T.; Camargo, P.; Xia, Y. N. *Nano Res.* **2010**, *3*, 69−80.
(25) Price, S. W. T.; Speed, J. D.; Kannan, P.; Russell, A. E. *J. Am. Chem. Soc.* **2011**, *133*, 19448−19458.
(26) Brimaud, S.; Behm, R. J. *J. Am. Chem. Soc.* **2013**, *135*, 11716−11719.
(27) Nørskov, J. K.; Rossmeisl, J.; Logadottir, A.; Lindqvist, L.; Kitchin, J. R.; Bligaard, T.; Jonsson, H. *J. Phys. Chem. B* **2004**, *108*, 17886−17892.
(28) Zhang, J.; Vukmirovic, M. B.; Xu, Y.; Mavrikakis, M.; Adzic, R. R. *Angew. Chem., Int. Ed* **2005**, *44*, 2132−2135.

(29) Greeley, J.; Stephens, I. E. L.; Bondarenko, A. S.; Johansson, T. P.; Hansen, H. A.; Jaramillo, T. F.; Rossmeisl, J.; Chorkendorff, I.; Nørskov, J. K. *Nat. Chem.* **2009**, *1*, 552−556.
(30) Stamenkovic, V.; Mun, B. S.; Mayrhofer, K. J. J.; Ross, P. N.; Markovic, N. M.; Rossmeisl, J.; Greeley, J.; Norskov, J. K. *Angew. Chem., Int. Ed.* **2006**, *45*, 2897−2901.
(31) Xiao, L.; Huang, B.; Zhuang, L.; Lu, J. T. *RSC Adv.* **2011**, *1*, 1358−1363.
(32) Wang, G. W.; Xiao, L.; Huang, B.; Ren, Z. D.; Tang, X.; Zhuang, L.; Lu, J. T. *J. Mater. Chem.* **2012**, *22*, 15769−15774.
(33) *FY12 Annual Progress Report for the DOE Hydrogen and Fuel Cells Program*; U.S. Department of Energy: Washington, D.C., December 2012, http://www.hydrogen.energy.gov/annual_progress12.html.
(34) Kresse, G.; Furtmüller, J. *Comput. Mater. Sci.* **1996**, *6*, 15−50.
(35) Kresse, G.; Furtmüller, J. *Phys. Rev. B* **1996**, *54*, 11169−11186.
(36) Hammer, B.; Hansen, L. B.; Norskov, J. K. *Phys. Rev. B* **1999**, *59*, 7413−7421.
(37) Monkhorst, H. J.; Pack, J. D. *Phys. Rev. B* **1976**, *13*, 5188−5192.
(38) Stamenkovic, V.; Mun, B. S.; Mayrhofer, K. J. J.; Ross, P. N.; Markovic, N. M.; Rossmeisl, J.; Greeley, J.; Nørskov, J. K. *Angew. Chem., Int. Ed.* **2006**, *118*, 2963−2967.
(39) Strasser, P.; Koh, S.; Anniyev, T.; Greeley, J.; More, K.; Yu, C.; Liu, Z.; Kaya, S.; Nordlund, D.; Ogaswawra, H.; Toney, M. F.; Nilsson, A. *Nat. Chem.* **2010**, *2*, 454−460.
(40) Lima, F. H. B.; Zhang, J.; Shao, M. H.; Sasaki, K.; Vukmirovic, M. B.; Ticianelli, E. A.; Adzic, R. R. *J. Phys. Chem. C* **2007**, *111*, 404−410.
(41) Henry, J.; Maljusch, A.; Huang, M.; Schuhmann, W.; Bondarenko, A. *ACS Catal.* **2012**, *2*, 1457−1460.
(42) Wang, S.; Jiang, S. P.; Wang, X.; Guo, J. *Electrochim. Acta* **2011**, *56*, 1563−1569.
(43) Shao, M. H.; Shoemaker, K.; Peles, A.; Kaneko, K.; Protsailo, L. *J. Am. Chem. Soc.* **2010**, *132*, 9253−9255.
(44) Maillard, F.; Schreier, S.; Hanzlik, M.; Savinova, E. R.; Weinkauf, S.; Stimming, U. *Phys. Chem. Chem. Phys.* **2005**, *7*, 385−393.
(45) The ratio between surface areas calculated from CO-stripping and H-upd charge is 1.5 for Pt^{s}AuCu *i*NPs and 1.1 for Pt/C. The H-upd charge was not used for surface area calculation in the present work because the integration of the H-upd charge has to be done on a slowly going curve superposed by the H_2 evolution, leading to greater error and usually underestimation of the surface area.
(46) Zhao, D.; Xu, B. Q. *Angew. Chem., Int. Ed.* **2006**, *45*, 4955−4959.
(47) Mayrhofer, K. J. J.; Blizanac, B. B.; Arenz, M.; Stamenkovic, V. R.; Ross, P. N.; Markovic, N. M. *J. Phys. Chem. B* **2005**, *109*, 14433−14440.
(48) Wang, C.; Chi, M.; Li, D.; Strmcnik, D.; van der Vliet, D.; Wang, G.; Komanicky, V.; Chang, K.-C.; Paulikas, A. P.; Tripkovic, D.; Pearson, J.; More, K. L.; Markovic, N. M.; Stamenkovic, V. R. *J. Am. Chem. Soc.* **2011**, *133*, 14396−14403.
(49) Yasuda, H.; Mori, H. Z. *Phys. D* **1996**, *37*, 181−186.